Research Article

Remote laser ablation electrospray ionization mass spectrometry for non-proximate analysis of biological tissues

Laine R. Compton[1], Brent Reschke[2], Jordan Friend[2], Matthew Powell[2] and Akos Vertes[1]*

[1]Department of Chemistry, W.M. Keck Institute for Proteomics Technology and Applications, The George Washington University, Washington, DC 20052, USA
[2]Protea Biosciences, 955 Hartman Run Road, Morgantown, WV 26505, USA

RATIONALE: We introduce remote laser ablation electrospray ionization (LAESI), a novel, non-proximate ambient sampling technique. Remote LAESI allows additional analytical instrumentation to be incorporated during sample analysis. This work demonstrates the utility of remote LAESI and, when combined with optical microscopy, allows for the microscopy-guided sampling of biological tissues.

METHODS: Rapid prototyping using a 3D printer was applied to produce various ablation chamber geometries. A focused 5 ns, 2.94 μm laser pulse kept at 10 Hz ablated the sample within the chamber, remote to the mass spectrometer inlet. Ablated particulates were carried through a transfer tube by N_2 gas, delivered to the electrospray plume and ionized. A long-distance microscope was used to capture images of tissues before, during and after ablation.

RESULTS: Optimized remote LAESI was found to have a 27% transport efficiency compared with conventional LAESI, sufficient for many applications. A comparable molecular coverage was obtained with remote LAESI for the analysis of plant tissue. Proof-of-principle experiments using a pansy flower and a maple leaf indicated the functionality of this approach for selecting domains of interest for analysis by optical microscopy and obtaining chemical information from those selected regions by remote LAESI-MS.

CONCLUSIONS: Remote LAESI is an ambient non-proximate sampling technique, proven to detect metabolites in biological tissues. When combined with optical microscopy, remote LAESI allows for the simultaneous acquisition of morphological and chemical information. This technique has important implications for histology, where chemical information for specific locations within a tissue is critical. Copyright © 2014 John Wiley & Sons, Ltd.

The analysis of biological tissues provides important insights into the organization and functioning of complex living organisms. Often, the need for chemical information is essential for the investigation of biological tissues, especially for the comparison of normal and abnormal or diseased regions within a tissue (e.g., surgical margins). This demands methodologies that are highly sensitive, specific and accurate. Mass spectrometry (MS) has become an important tool for the investigation of biological tissues due to the low limits of detection, variety of instrumentation and the ability to measure multiple compounds within a highly complex sample.

Matrix-assisted laser desorption/ionization (MALDI) is the most common MS method used to study biological tissues, specifically for chemical imaging purposes. In MALDI-MS, the tissue must be treated with a small organic acid matrix prior to analysis.[1] However, the use of matrix compounds to facilitate desorption and ionization introduces spectral interferences in the lower *m/z* range, hindering the detection of metabolites and other lower molecular weight compounds.[2]

The discovery of ambient ionization, pioneered by desorption electrospray ionization (DESI), eliminated the need for sample pretreatment or a matrix and has been an important development for *in situ*, *in vivo* and *ex vivo* analyses of biological samples.[3–8]

Since the introduction of DESI, many other ambient ion sources have been developed,[4] including direct analysis in real time (DART)[9] and laser ablation electrospray ionization (LAESI).[10] To maximize sensitivity, ambient ionization techniques typically analyze samples in the immediate vicinity of the mass spectrometer inlet orifice. As with most ambient sampling methods, LAESI-MS requires the laser ablation and ionization events to occur within a few cm of the inlet orifice.[10] This geometrical requirement prevents the incorporation of additional analytical instrumentation (e.g., fluorescence microscopy) to be utilized during analysis. This constraint leads to the need for a remote sampling device to transfer the particulates generated by laser ablation to the electrospray ionization source and mass spectrometer.

Ambient mass spectrometry techniques that employ remote sampling devices include laser ablation inductively coupled plasma (LA-ICP),[11,12] remote DESI[13–15] and remote analyte sampling, transport and ionization relay (RASTIR).[16] A new modality of DESI, termed nano-DESI, has recently demonstrated the combination of a sampling capillary and an

* *Correspondence to:* A. Vertes, Department of Chemistry, The George Washington University, 725 21-st Street, N.W., Washington, DC 20052, USA.
E-mail: vertes@gwu.edu

inverted microscope to both visualize and analyze mouse tissue sections, allowing for selection of particular regions of a tissue section for analysis.[17] Similarly, a laser ablation (LA) atmospheric pressure chemical ionization (APCI) MS technique was developed where ablated particulates were carried through a Teflon® tube to a sampling capillary for APCI. The LA-APCI method was also combined with brightfield and fluorescence microscopy to correlate chemical and spatial information.[18] The aforementioned techniques were used to successfully examine the composition of biological tissues and compounds on elemental and molecular levels.[12,14,16–18]

Due to the potential synergism of the obtained morphological and chemical information, the combination of optical microscopy with laser ablation is a compelling new modality for LAESI. Here, we present remote LAESI-MS where the laser ablation event takes place in a chamber sufficiently removed from the front of the mass spectrometer to accommodate an optical microscope. An ablation plume is generated by a pulsed, nanosecond mid-IR wavelength laser inside the chamber. Ablated particulates are transported through a transfer tube by N_2 carrier gas and delivered to the electrospray for ionization. In this article, proof-of-principle experiments are presented for remote LAESI, including comparisons with conventional LAESI and the demonstration of non-proximate microscopy-guided tissue sampling.

EXPERIMENTAL

Chemicals and biological samples

HPLC-grade methanol and water were purchased from Alfa Aesar (Ward Hill, MA, USA). Verapamil hydrochloride and acetic acid were purchased from Sigma Aldrich (St. Louis, MO, USA) and stock solutions were prepared in HPLC-grade water.

The two species from the *Viola* genus (a generic violet and a hybrid, also known as pansy) and maple (*Acer* spp.) leaf samples were obtained from the George Washington University campus (Washington, DC, USA). Selected sections of the plant tissues were cut into 1 cm × 2 cm rectangles immediately before analysis and affixed to the bottom of the ablation chamber or a glass microscope slide using double-sided tape.

Ablation chambers

To test a variety of ablation chamber geometries, rapid prototyping aided by a three-dimensional (3D) printer was implemented. The chambers were made of acrylonitrile butadiene styrene (ABS) material (ABSM30). The chambers were printed with a Fortus 400 mc printer, using a T10 tip to print the ABS. The support material was SR30 and it was printed with a T12SR20/30 tip. After printing, the support material was removed sonication for 2 h in a bath of WaterWorks soluble concentrate (P4000SC). The printer, ABS plastic, support material, tips and WaterWorks concentrate were all purchased from Stratasys (Eden Prairie, MN, USA).

The ablation chamber consisted of three essential components: a cover, an adjustable spacer and a platform (see Supplementary Fig. S1, Supporting Information). Affixed to the ablation chamber cover was a transparent CaF_2 optical quality window (WG1050, Thorlabs, Newton, NJ, USA). The produced and tested chamber cavities covered a volume range between 5 cm^3 and 75 cm^3 and included prolate spheroid and elliptic cylinder inner geometries. The chamber platform consisted of ABS with a recessed area to accommodate a microscope slide for mounting the sample. The ablation chamber cover, spacer and platform were held together by four stainless steel screws.

A 60 cm long polytetrafluoroethylene (PTFE) tube (4 mm i.d.) was used to transfer the ejected sample plume from the ablation chamber to the electrospray in front of the mass spectrometer inlet orifice. Nitrogen carrier gas at 0.1–2.0 L/min flow rates, regulated by a gas flow meter (Key Instruments, Trevose, PA, USA), entrained the aerosol of the ablated material from the ablation chamber into the transfer tube.

Laser ablation and optical microscopy

The primary challenge for the optical system was the simultaneous delivery of the ablating laser pulses at 2940 nm in the mid-IR wavelength range to the focusing lens, and the microscope observation and image acquisition in the visible range using the same lens. In laser ablation systems this is typically achieved by the combination of the two beams using a dichroic mirror at 45° to the sample surface normal that reflects the ablating light and transmits in the visible region. Although there was no ideal off-the-self solution available, the selected shortpass dichroic mirror (DMSP805, Thorlabs) had ~95% transmission in the visible range and ~20% reflectance at the 2940 nm wavelength used for ablation. The transmitted mid-IR radiation behind the mirror was stopped by a beam block. The focusing element consisted of a CaF_2 plano-convex lens with 150 mm focal length (LA5012, Thorlabs) or, for smaller chambers, an infinity corrected reversed Cassegrain microscope objective in the Schwarzschild configuration (50105-02, Newport, Franklin, MA, USA) with a 24 mm working distance. The advantage of this reflective objective is that it is free of chromatic aberration due to its nearly wavelength-independent performance in the mid-IR region, and it exhibits negligible spherical aberrations.

For both remote and conventional LAESI, 2.94 μm wavelength laser radiation was produced at 10 Hz repetition rate by a Nd:YAG laser driven optical parametric oscillator (Opolette 100, Opotek, Carlsbad, CA, USA) with 2.6 ± 0.1 mJ pulse energy. The laser beam was steered to the dichroic mirror and the focusing lens by two gold-coated mirrors (PF10-03-M01, Thorlabs).

For optical microscopy, a tube lens (MT-1, Edmund Optics, Barrington, NJ, USA) combined with a zoom lens (Optem Zoom 70XL, Qioptic, Rochester, NY, USA) projected the visible radiation transmitted through the dichroic mirror onto the camera. Images were acquired using a CMOS color camera (Marlin F131, Allied Vision Technologies, Stadtroda, Germany). The field of view of the camera was aligned to contain the focal spot of the laser beam. Figure 1 depicts a schematic representation of the experimental arrangement for remote LAESI-MS coupled with optical microscopy.
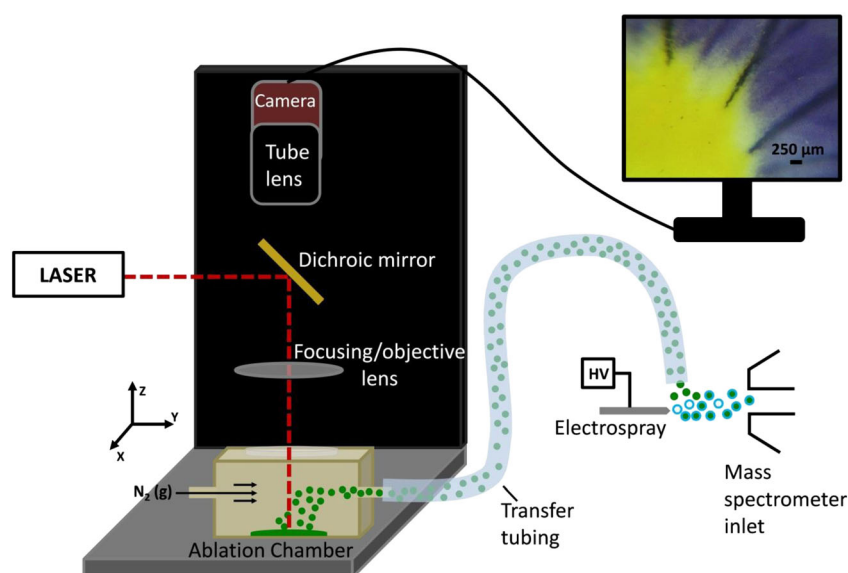
Figure 1. Schematic of the remote LAESI experimental setup. A 2.94 μm laser beam is deflected by a dichroic mirror and focused through a lens. To observe the sample within the chamber, a tube lens collects the visible light transmitted through the dichroic mirror. Ablated particulates (represented by solid green circles) travel through a transfer tube carried by N_2 gas, become entrained and are ionized in the electrospray plume (droplets indicated by blue rings) before entering the mass spectrometer inlet orifice.

Electrospray and mass spectrometer

A home-built electrospray source, as described previously,[10] was used in both the conventional and the remote LAESI experiments. Briefly, the electrospray was produced by pumping a 50% methanol solution acidified with 0.1% acetic acid (v/v) through a stainless steel emitter (MT320-100-5-5, i.d. 100 μm, New Objective, Woburn MA, USA) by a syringe pump (SP100I World Precision Instruments, Sarasota, FL, USA) at 0.400 μL/min flow rate. High voltage (+2.8–3.4 kV) applied to the emitter was generated by a stable power supply (PS350, Sanford Research Systems, Sunnyvale, CA, USA). The emitter was placed on axis with the center of the mass spectrometer inlet orifice at a distance of 1 cm.

Data was acquired in positive ion mode using a Q-TOF Premier mass spectrometer (Waters Co., Milford, MA, USA) and processed using MassLynx (Waters Co.) and Origin 8.5 (OriginLab Corporation, Northampton, MA, USA) software programs.

RESULTS AND DISCUSSION

Rapid prototyping of the ablation chamber

To explore a variety of chamber geometries, numerous configurations were printed. We varied the height and the inner volume of the chambers, the shape of the cavity, the diameters of the inlet and outlet gas ports and measured the corresponding ion signal generated from 100 μM verapamil solution standards. Initially, the volume of the cavity was varied by inserting a spacer at the middle of the chamber body. Improved results were observed when a prolate spheroid chamber (with a $2b = 31$ mm major axis, a $2a = 25$ mm

minor axis and $V_1 = 4\pi a^2 b/3 = 10.1$ cm^3 volume) was modified by introducing a $h = 9$ mm high elliptic cylinder spacer resulting in a 34 mm distance between the sample and the chamber cover. The spacer increased the volume of the chamber by $V_2 = \pi abh = 5.4$ cm^3 to $V = V_1 + V_2 = 15.5$ cm^3.

To avoid hitting the top of the chamber, the ablated particles have to be slowed down sufficiently by the drag force and entrained by the carrier gas flow. If the carrier gas flow is parallel with the ablated surface and the ablated particles start out with a v_0 velocity perpendicular to the surface, the stopping distance in that direction, x_{stop}, of a particle with a diameter of $2R$ is $x_{stop} = 2\rho R^2 v_0/9\mu$, where ρ and μ are the density of the particle and the dynamic viscosity of the carrier gas, respectively.[19] The 34 mm space available for particulate ejection in the optimized chamber is consistent with the calculated stopping distance for water droplets of 8.4 μm diameter in resting ambient air. This means that most particles of this size and smaller do not reach the top of the chamber and are likely to be entrained by the carrier gas flow.

After extensive testing of the shape of the cavity, the best performing geometries (prolate spheroid and elliptic cylinder) were selected for further investigation. These studies yielded superior signal intensities for the prolate spheroid ablation chamber in remote LAESI experiments.

Subsequently, the carrier gas flow rate, length and inner diameter of the transfer tube and the positioning of its outlet with respect to the electrospray emitter and the mass spectrometer inlet orifice were systematically varied to obtain maximum ion yields. Using aqueous verapamil solutions as the sample, it was found that 0.5–1 L/min gas flow rates, a 4 mm i.d. transfer tube, and the delivery of the transported aerosol 0.5–1 cm above and at a right angle with respect to the tip of the electrospray emitter resulted in increased ion production. In these experiments, we verified that the ion

signal produced by the setup was correlated with the laser ablation by monitoring it in the presence and absence of laser action. Carrier gas flow rates greater than 1 L/min tended to displace the sample in the chamber. A 60 cm tube length was selected as a tradeoff that allowed sufficient distance from the mass spectrometer for the incorporation of the optical microscope but was short enough to have acceptable transport efficiency.

To minimize transportation losses in the ablation chamber and transfer tube, laminar gas flow throughout the entire system is desirable. The Reynolds number (*Re*), $Re = \rho v D/\mu$, can be used to distinguish the flow regimes within the plume transport system, where ρ is the fluid density, v is the linear velocity, D is the critical dimension of the flow, i.e., the dimension of the narrowest point for the ablation chamber and the i.d. for the transfer tube, and μ is the dynamic viscosity. For tube geometry, the transition from laminar to sustained turbulent flow is established as $Re \approx 2040$.[20] Using the density and dynamic viscosity of the nitrogen carrier gas, a carrier gas flow rate of 1 L/min and assuming that the contribution of the ablation plume was negligible relative to those two values, the Reynolds numbers for the ablation chamber and the transfer tube were 1416 and 354, respectively. These numbers are well below the critical Reynolds number of 2040, indicating a laminar flow regime.

Among the studied geometrical parameters, the position of the aerosol delivery with respect to the electrospray plume and mass spectrometer inlet, depicted in Fig. 1, seemed to have the most influence on the obtained ion intensities. Setting a 1–2 mm distance between the transfer tube opening and the tip of the electrospray emitter resulted in significantly increased ion signal.

Remote vs conventional LAESI

To determine the transport efficiency in remote LAESI, we compared verapamil ion intensities for a range of sample solution concentrations with those resulting from conventional LAESI. For the analysis, 10 µL aliquots of verapamil solutions with concentrations down to 0.1 µM were deposited on the bottom of the ablation chamber and entirely ablated. The ablation chamber and transfer tube were thoroughly cleaned between the measurements to avoid carry-over between samples. Similarly, 10 µL aliquots of the verapamil solutions were deposited on a glass microscope slide and completely ablated for conventional LAESI experiments.

Using the optimal parameters that provided the highest ion intensities as discussed above, a limit of detection for remote LAESI was established as 5.0 pmol for verapamil analyte (see Fig. 2) and a dynamic range of over two orders of magnitude was observed. Linear regression for the remote LAESI data indicated a correlation coefficient of 0.98. The inset in Fig. 2 shows that the signal-to-noise ratio for the protonated verapamil peak (*m/z* 455.290) at the limit of detection is greater than 3.

Compared with conventional LAESI, the remote technique demonstrated ~27% signal strength, calculated based on the ratios of the verapamil ion intensities for several concentrations. The losses can be attributed to transient turbulences in the gas flow within the ablation chamber,
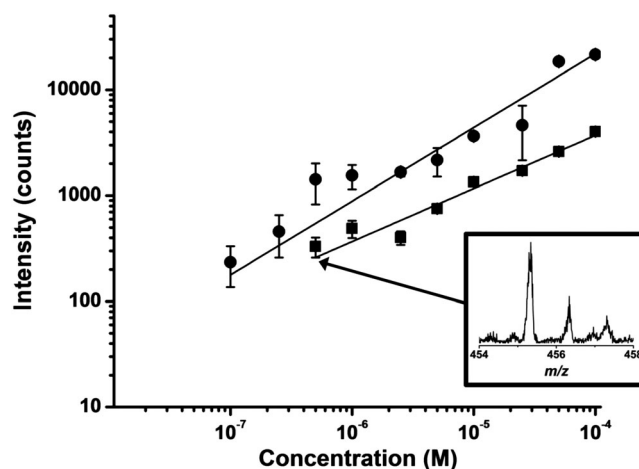
Figure 2. Ion intensities from 10 µL verapamil solution as a function of concentration measured by conventional (●) and remote (■) LAESI. The inset indicates a signal-to-noise ratio greater than 3 at the limit of detection for remote LAESI.

radial diffusion inside the transfer tube, settling of larger particulates, and incomplete ionization of the delivered ablation products by the electrospray plume.

To ensure that the molecular coverage obtained by remote LAESI was similar to that of the conventional technique, the purple pigmented region of a violet petal was sampled by both LAESI modalities and the spectra were compared. Twenty spectra were averaged and background subtracted for both conventional and remote LAESI and the resulting spectra were compared (see Fig. 3). An image of the violet flower is shown in the inset of Fig. 3, with a dashed circle indicating the region of petal analysis. Compared with conventional LAESI, reduced signal intensity was observed for remote LAESI, whereas the molecular coverage remained similar. The total number of peaks, excluding isotope distributions, obtained by remote LAESI was 96, whereas, for conventional LAESI, 123 peaks were seen. The
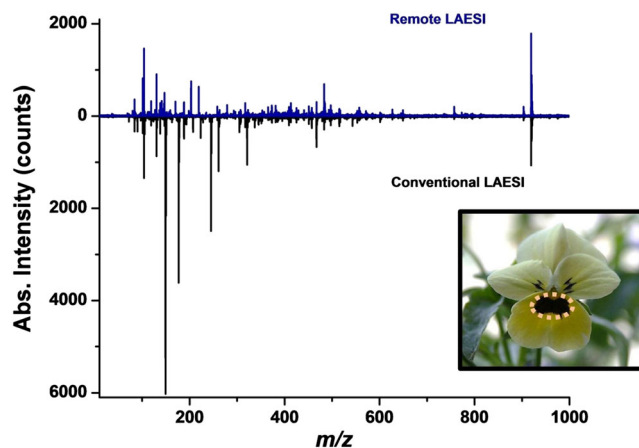
Figure 3. Mass spectra resulting from the purple pigmented region of a violet flower petal for conventional LAESI (▬) (bottom) and remote LAESI (▬) (top). An optical image of the flower is shown in the inset. Remote LAESI demonstrates a molecular coverage comparable with the conventional technique. Some of the variation between the spectra is due to biological heterogeneity.

comparable molecular coverage along with the somewhat lower dynamic range are important attributes of remote LAESI for the characterization of biomedical samples.

Remote LAESI with optical microscopy

To demonstrate the application of remote LAESI combined with optical microscopy, a section of a pansy flower petal showing two distinctively colored regions, purple and yellow, was carefully excised and mounted inside the ablation chamber (see Fig. 4(a)). Observation of the sample through the microscope assisted in targeting the regions for analysis. The mass spectra of the purple and yellow regions of the petal were consecutively acquired (see Figs. 4(c) and 4(d), respectively).

The optical image of the pansy petal section following the ablations is shown in Fig. 4(b). The m/z 700–1000 range in the mass spectra is magnified ten times to show some of the ions that were different within the two petal regions (a few of them are indicated by asterisks for the purple region and diamonds for the yellow region).

In the purple region, the m/z 919.251 ion was identified by tandem mass spectrometry (MS/MS) as protonated delphinidin-coumaroyl-rutinoside-glucoside, a flavonoid pigment commonly associated with purple plant tissues (see Supplementary Fig. S2, Supporting Information).[21,22] The ion at m/z 757.220 corresponds to the deglycosylation of the flavonoid observed at m/z 919.251. Some of the peaks shared between the two petal sections are m/z
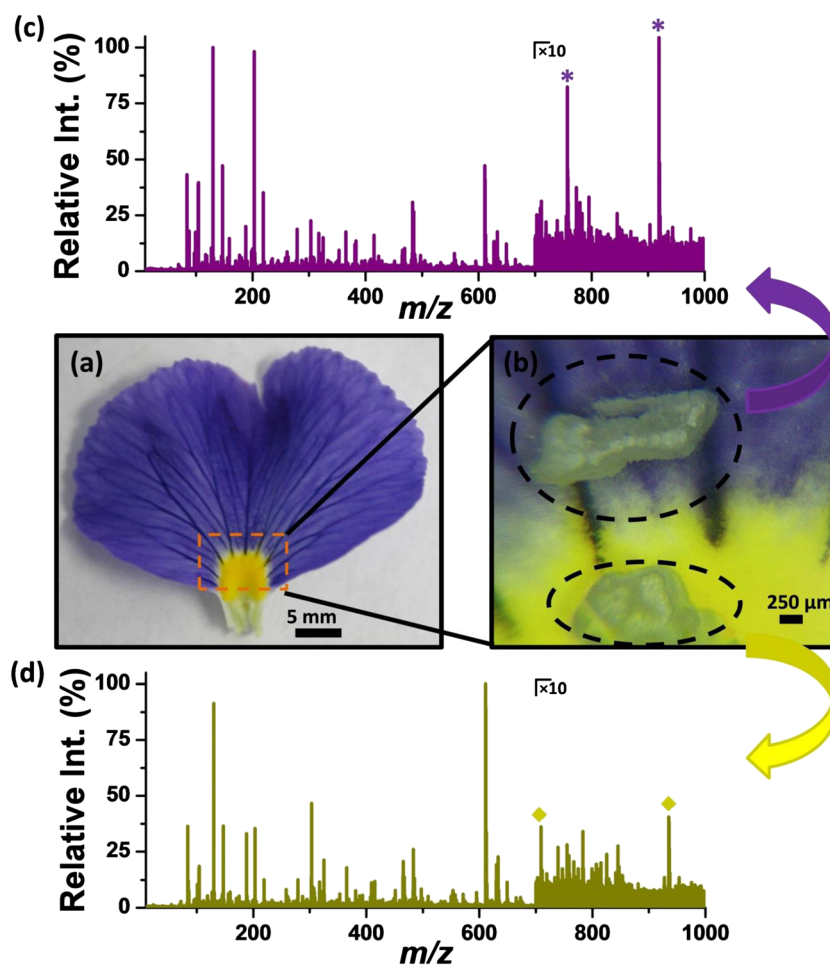

Figure 4. Local analysis of differently colored areas in flower petal by remote LAESI combined with optical microscopy. (a) Optical image of pansy petal, (b) microscope image of two ablated regions inside ablation chamber, (c) remote LAESI mass spectrum corresponding to the purple region with a few ions, unique to the region, indicated by (∗), and (d) remote LAESI mass spectrum corresponding to the yellow region with a few specific ions indicated by (◆). The regions between m/z 700 and 1000 are magnified ten times to show key differences in the two spectra to show key differences. Ions with an m/z 919.251 and 757.220 were identified as protonated delphinidin-coumaroyl-rutinoside-glucoside and protonated delphinidin-coumaroyl-glucoside, respectively, using tandem MS measurements (see Fig. S2 in the Supporting Information). They only appeared in the purple region of the petal. Ions with m/z 709.138 and 935.192 were only present in the yellow region of the petal.
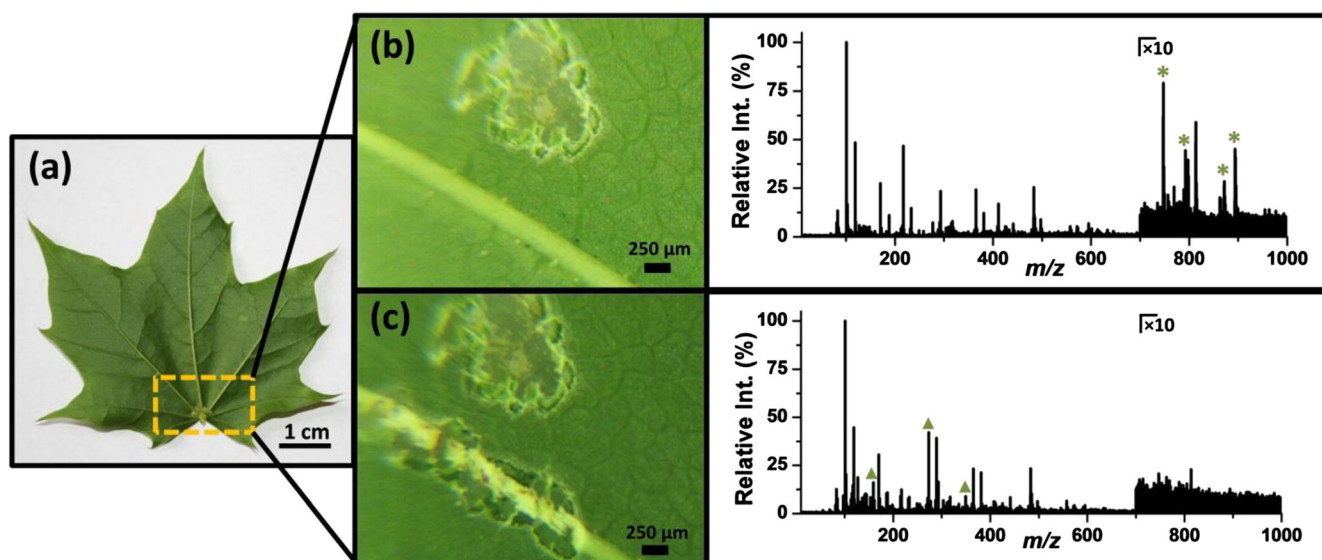
Figure 5. Profiling an area in a maple leaf using remote LAESI-MS. (a) Optical image of the maple leaf with a rectangle indicating the region of tissue selected for analysis, (b) microscope image of ablated leaf blade in the ablation chamber, and (c) microscope image of ablated vein segment in the ablation chamber. Corresponding remote LAESI mass spectra for the two areas are shown to the right of the microscope images. The range between *m/z* 700 and 1000 is magnified ten times to show the key spectral differences between the two tissue regions. Ions found exclusively and more abundantly in the blade portion of the leaf are indicated by (✳) and those in the vein are shown by (▲).

365.108 and 381.079, which are the sodium and potassium adduct ions of sucrose, and an unidentified ion at *m/z* 611.140. Unidentified ions specific to the yellow region include *m/z* 709.138 and 935.192.

We demonstrate the application of remote LAESI for microscopy-guided profiling of a maple leaf, sectioned to contain portions of the blade and vein, two distinctively different tissue types. Figure 5(a) shows an optical image of the backside of the leaf with the section used for sampling marked by a frame. The microscope images from inside the ablation chamber were obtained after the blade and vein regions were analyzed independently (see Figs. 5(b) and 5(c), respectively). The mass spectra for the two tissue types are shown to the right of the corresponding images. The *m/z* 700–1000 region is magnified ten times to show the presence of ions in this range.

As can be seen in Fig. 5(b), approximately 20 blade cells of the leaf were ablated. The blade of the leaf contained characteristic disaccharide ions (e.g., *m/z* 365.105 and 381.079 alkaline ion adducts of sucrose) as well as ions above *m/z* 700 specific to the blade. For example, the ion at *m/z* 893.543, present more abundantly in the blade, was identified as protonated chlorophyll *a* through MS/MS measurements (see Supplementary Fig. S3, Supporting Information). Additional ions, found only in the blade region of the leaf, were *m/z* 411.144, 747.211, 792.608 and 871.590.

A ~2 mm portion of the vein was analyzed using ablation sampling, as can be seen in Fig. 5(c). The vein exhibited similar ions to the leaf blade, such as the disaccharides mentioned above, yet showed low ion abundances in the higher *m/z* region. Some characteristic ions specific to the vein tissue type were found primarily in the lower mass region and included those at *m/z* 273.094, 289.075 and 291.077.

CONCLUSIONS

Conventional LAESI is a useful sampling and ambient ionization technique for the direct analysis of cells and biological tissues. The current geometrical limitations, however, prevent the incorporation of additional instrumentation to aid precise targeting of sample domains of interest for analysis. Here we have presented remote LAESI as a means to overcome the restrictions dictated by the configuration of the conventional modality. Using remote LAESI allows for optical visualization and targeting of small sample areas before, during and after laser ablation.

Compared with conventional LAESI, the remote technique has a somewhat reduced sensitivity and dynamic range that are still sufficient for the analysis and characterization of numerous metabolites and lipids in diverse spatial regions of biological tissues. Remote LAESI was utilized for the microscopy-guided sampling and comparative analysis of plant tissues. It was found that sample carry-over due to the transport of the ablated material did not affect subsequent measurements and representative mass spectra corresponding to selected regions of interest were obtained.

Future efforts to improve the sensitivity might seek to characterize the flow dynamics within the ablation chamber. Modifications to the gas dynamic transport and integration of additional devices (e.g., aerodynamic amplifiers and merging devices) may help to improve the transport efficiency and consequently the overall sensitivity of remote LAESI. Rapid prototyping, based on 3D printing, will accelerate the testing of additional geometries for the ablation chambers with improved entrainment of the ablation plume into the transfer gas stream.

The development of remote LAESI demonstrates the utility of microscope visualization when analyzing biological tissues in an ambient setting. Remote LAESI-MS opens the door for histological applications, where site-specific sampling and analysis are essential for sample characterization.

Acknowledgements

REFERENCES

[1] E. H. Seeley, R. M. Caprioli. MALDI imaging mass spectrometry of human tissue: method challenges and clinical perspectives. *Trends Biotechnol.* **2011**, *29*, 136.

[2] J. C. Vickerman. Molecular imaging and depth profiling by mass spectrometry-SIMS, MALDI or DESI? *Analyst* **2011**, *136*, 2199.

[3] M. E. Monge, G. A. Harris, P. Dwivedi, F. M. Fernández. Mass spectrometry: Recent advances in direct open air surface sampling/ionization. *Chem. Rev.* **2013**, *113*, 2269.

[4] G. A. Harris, A. S. Galhena, F. M. Fernández. Ambient sampling/ionization mass spectrometry: Applications and current trends. *Anal. Chem.* **2011**, *83*, 4508.

[5] P. Nemes, A. Vertes. Ambient mass spectrometry for in vivo local analysis and in situ molecular tissue imaging. *Trac Trends Anal. Chem.* **2012**, *34*, 22.

[6] D. J. Weston. Ambient ionization mass spectrometry: current understanding of mechanistic theory; analytical performance and application areas. *Analyst* **2010**, *135*, 661.

[7] Z. Takáts, J. M. Wiseman, B. Gologan, R. G. Cooks. Mass spectrometry sampling under ambient conditions with desorption electrospray ionization. *Science* **2004**, *306*, 471.

[8] B. Shrestha, A. Vertes. High-throughput cell and tissue analysis with enhanced molecular coverage by laser ablation electrospray ionization mass spectrometry using ion mobility separation. *Anal. Chem.* **2014**, *86*, 4308.

[9] R. B. Cody, J. A. Laramée, H. D. Durst. Versatile new ion source for the analysis of materials in open air under ambient conditions. *Anal. Chem.* **2005**, *77*, 2297.

[10] P. Nemes, A. Vertes. Laser ablation electrospray ionization for atmospheric pressure, in vivo, and imaging mass spectrometry. *Anal. Chem.* **2007**, *79*, 8098.

[11] D. Bleiner, D. Gunther. Theoretical description and experimental observation of aerosol transport processes in laser ablation inductively coupled plasma mass spectrometry. *J. Anal. At. Spectrom.* **2001**, *16*, 449.

[12] B. Wu, J. S. Becker. Bioimaging of metals in rat brain hippocampus by laser microdissection inductively coupled plasma mass spectrometry (LMD-ICP-MS) using high-efficiency laser ablation chambers. *Int. J. Mass spectrom.* **2012**, *323*, 34.

[13] I. Cotte-Rodriguez, R. G. Cooks. Non-proximate detection of explosives and chemical warfare agent simulants by desorption electrospray ionization mass spectrometry. *Chem. Commun.* **2006**, 2968.

[14] I. Cotte-Rodríguez, C. C. Mulligan, R. G. Cooks. Non-proximate detection of small and large molecules by desorption electrospray ionization and desorption atmospheric pressure chemical ionization mass spectrometry: Instrumentation and applications in forensics, chemistry, and biology. *Anal. Chem.* **2007**, *79*, 7069.

[15] S. Garimella, W. Xu, G. Huang, J. D. Harper, R. G. Cooks, Z. Ouyang. Gas-flow assisted ion transfer for mass spectrometry. *J. Mass Spectrom.* **2012**, *47*, 201.

[16] R. B. Dixon, J. S. Sampson, A. M. Hawkridge, D. C. Muddiman. Ambient aerodynamic ionization source for remote analyte sampling and mass spectrometric analysis. *Anal. Chem.* **2008**, *80*, 5266.

[17] C.-C. Hsu, N. M. White, M. Hayashi, E. C. Lin, T. Poon, I. Banerjee, J. Chen, S. L. Pfaff, E. R. Macagno, P. C. Dorrestein. Microscopy ambient ionization top-down mass spectrometry reveals developmental patterning. *Proc. Natl. Acad. Sci. USA* **2013**, *110*, 14855.

[18] M. Lorenz, O. S. Ovchinnikova, V. Kertesz, G. J. Van Berkel. Laser microdissection and atmospheric pressure chemical ionization mass spectrometry coupled for multimodal imaging. *Rapid Commun. Mass Spectrom.* **2013**, *27*, 1429.

[19] P. Nemes, H. Huang, A. Vertes. Internal energy deposition and ion fragmentation in atmospheric-pressure mid-infrared laser ablation electrospray ionization. *Phys. Chem. Chem. Phys.* **2012**, *14*, 2501.

[20] K. Avila, D. Moxey, A. de Lozar, M. Avila, D. Barkley, B. Hof. The onset of turbulence in pipe flow. *Science* **2011**, *333*, 192.

[21] A. Soto-Vaca, A. Gutierrez, J. N. Losso, Z. M. Xu, J. W. Finley. Evolution of phenolic compounds from color and flavor problems to health benefits. *J. Agric. Food. Chem.* **2012**, *60*, 6658.

[22] J. Zhang, L. S. Wang, J. M. Gao, Y. J. Xu, L. F. Li, C. H. Li. Rapid separation and identification of anthocyanins from flowers of *Viola yedoensis* and *V. prionantha* by high-performance liquid chromatography-photodiode array detection-electrospray ionisation mass spectrometry. *Phytochem. Anal.* **2012**, *23*, 16.

SUPPORTING INFORMATION

Additional supporting information can be found in the online version of this article at the publisher's website.

Supporting Information for

Remote Laser Ablation Electrospray Ionization Mass Spectrometry for Non-proximate Analysis of Biological Tissues

Laine R. Compton,[1] Brent Reschke,[2] Jordan Friend,[2] Matthew Powell[2] and Akos Vertes[1]*

[1]Department of Chemistry, W.M. Keck Institute for Proteomics Technology and Applications, The George Washington University, Washington, DC 20052, USA

[2]Protea Biosciences, 955 Hartman Run Road, Morgantown, WV 26505, USA

*Correspondence to: Akos Vertes, Department of Chemistry, The George Washington University, 725 21-st Street, N.W., Washington, DC 20052, USA, Tel.: +1 (202) 994-2717; fax: +1 (202) 994-5873. E-mail address: vertes@gwu.edu
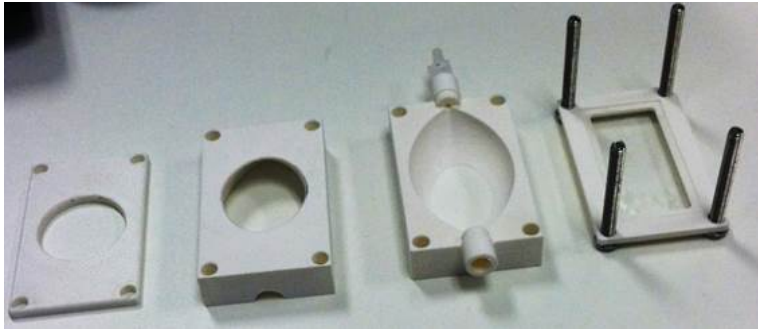
(a)   **(b)**

Figure S1. (a) Components of a remote ablation chamber produced by 3D printing. **(b)** Assembled remote ablation chamber without the IR window.
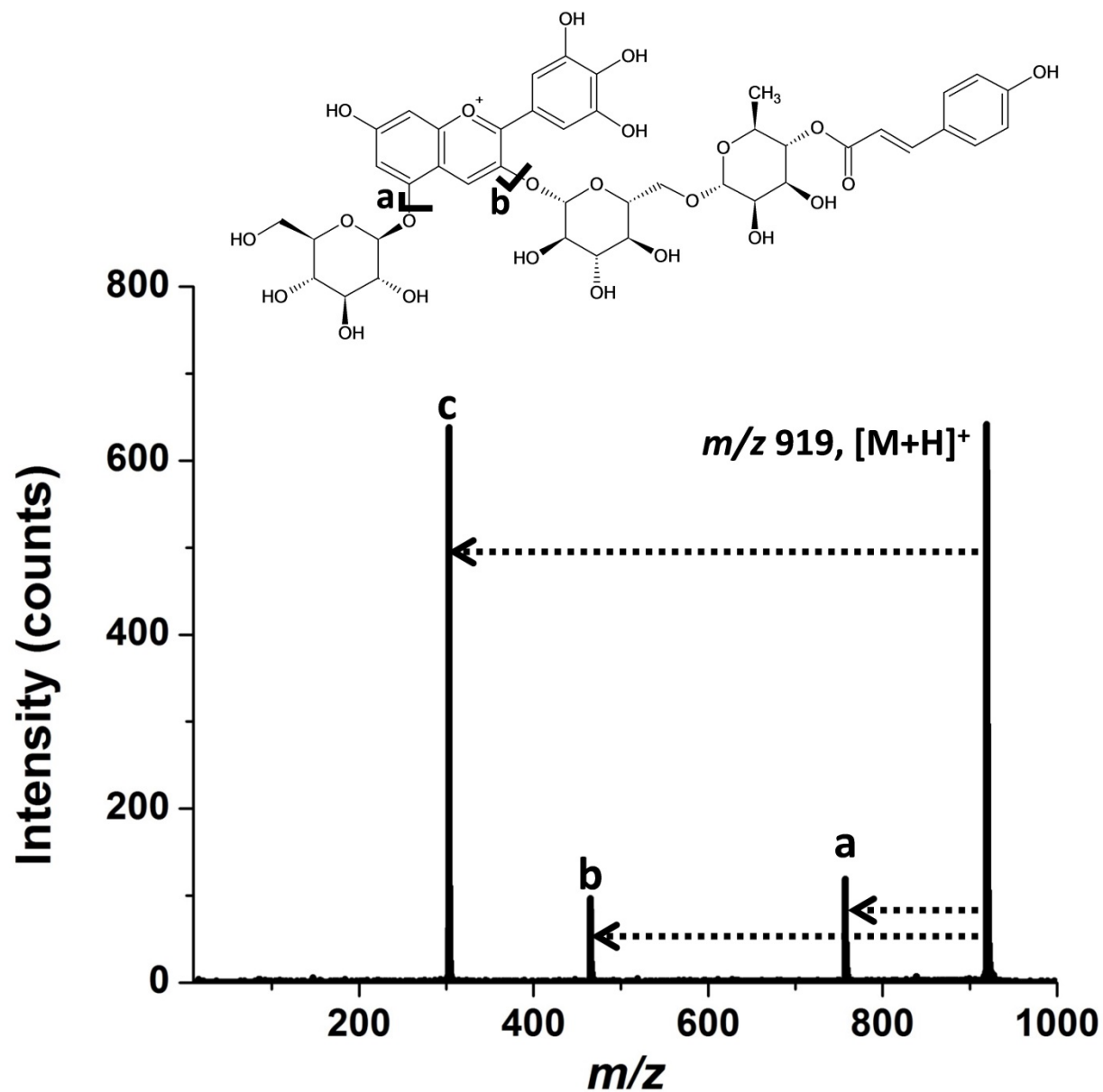
Figure S2. Tandem MS spectrum of the ion at nominal *m/z* 919. The fragmentation pattern corresponds to losses of glucose (labeled a), a diglucoside coumaroyl group (labeled b) and the delphinidin headgroup, labeled c.
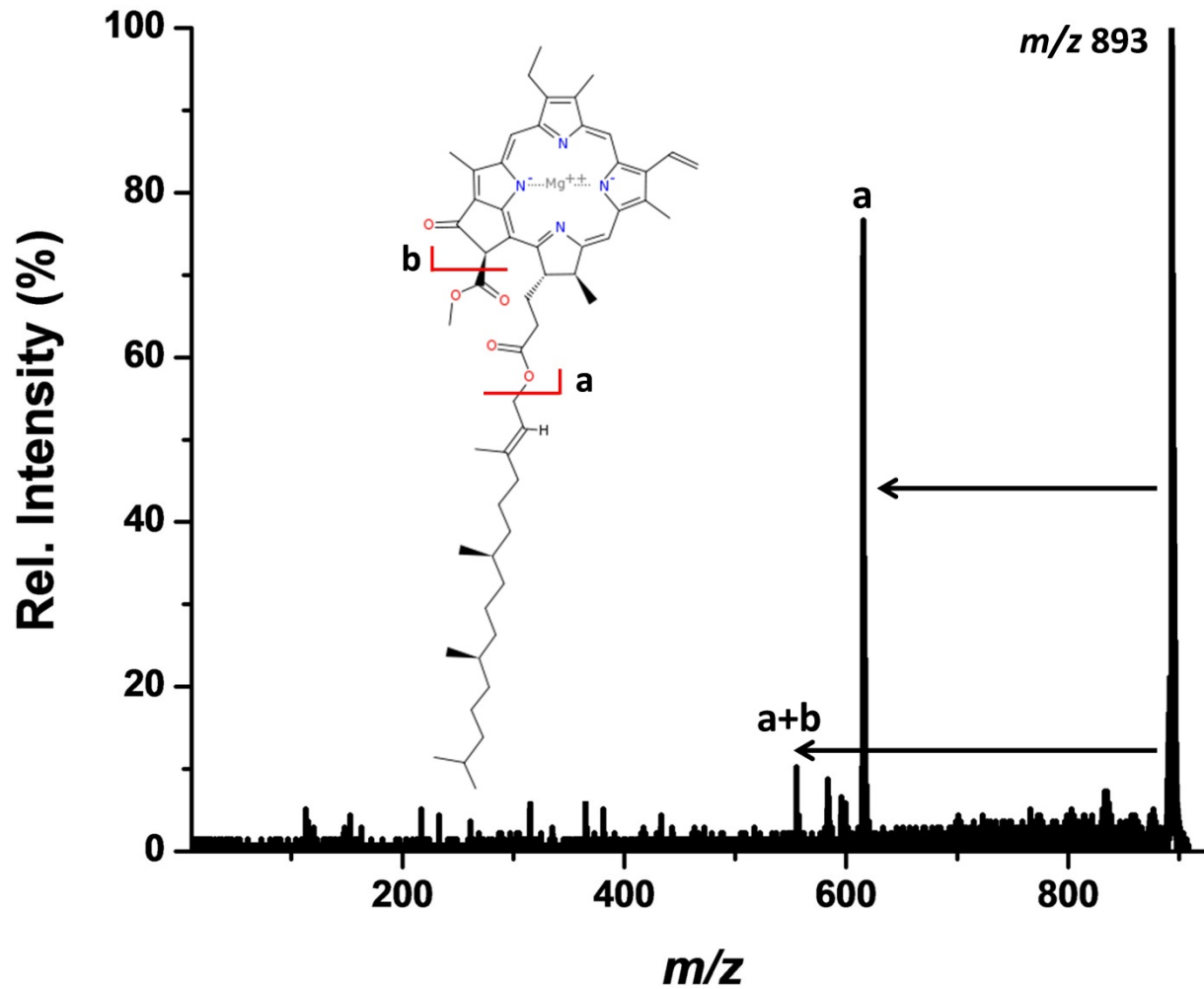
Figure S3. Tandem mass spectrum of the ion at nominal *m/z* 893 revealed fragments a and a+b that were consistent with a protonated chlorophyll *a* precursor ion.